Phase transitions in the ferroelastic $[P(CH_3)_4]SbCl_6$ crystal

1998 J. Phys.: Condens. Matter 10 5439

(http://iopscience.iop.org/0953-8984/10/24/020)

J. Phys.: Condens. Matter **10** (1998) 5439–5447. Printed in the UK PII: S0953-8984(98)90225-9

Phase transitions in the ferroelastic $[P(CH_3)_4]SbCl_6$ crystal

P Ciąpała†, R Jakubas†, G Bator†, A Pietraszko‡ and B Kosturek§

† Faculty of Chemistry, University of Wrocław, F Joliot-Curie 14, 50-383 Wrocław, Poland
‡ Institute of Low Temperature and Structure Research of the Polish Academy of Science, Okólna 2, 50-422 Wrocław, Poland
§ Institute of Experimental Physics, University of Wrocław, 9 Max Born Square, 50-204 Wrocław, Poland

Received 29 December 1997, in final form 20 March 1998

Abstract. Differential scanning calorimetry, dilatometric, dielectric and linear birefringence measurements have been used to study the ferroelastic $[P(CH_3)_4]SbCl_6$ crystal. It was found that the crystal undergoes two structural phase transitions, at 350 K (second order) and at 405 K (first order). The x-ray temperature studies showed that at 350 K the crystal changes its symmetry from triclinic $P\bar{1}$ to monoclinic $C2/m$. Ferroelastic domain structure was found in the room temperature phase (below 350 K).

1. Introduction

Halogenoantimonate(V) salts containing organic cations belong to a large family of molecular–ionic crystals. Up to now, only the fluoroantimonate analogues, such as $[N(CH_3)_4]SbF_6$ and $[N(C_2H_5)_4]SbF_6$, have been systematically studied, using x-ray [1], NMR [2, 3] and spectroscopic (IR and Raman) [4–6] techniques. The two compounds just named revealed dynamical disorder of both the SbF_6 octahedral and the cationic units. The low-temperature phase transitions in the fluoroantimonate(V) salts are triggered by cation and anion motion. The knowledge of the physical properties of the chloroantimonate(V) salts is quite poor. Recently, we studied a new crystal from this family, of the formula $[C(NH_2)_3]SbCl_6$ (GCA) [7]. This crystal undergoes structural phase transitions at 351 and 265 K. One of the two crystallographically inequivalent $SbCl_6^-$ anions disordered at room temperature was postulated to contribute to the phase transition mechanism at 265 K. It was found that GCA was ferroelastic below 351 K. In a search for other members of the ferroelastic family of chloroantimonate(V) salts, we have chosen tetramethylphosphonium chloroantimonate(V), $[P(CH_3)_4]SbCl_6$ (TMPCA), for further study. This paper is devoted to preliminary x-ray, differential scanning calorimetry (DSC), dielectric, birefringence and optical results for a new ferroelastic TMPCA crystal.

2. Experimental details

The crystal of $[P(CH_3)_4]SbCl_6$ was synthesized by reacting $P(CH_3)_4Cl$ and $SbCl_5$ in an aqueous solution, and the single crystal was grown by the evaporation method at room temperature from an ethanol solution.

The x-ray diffraction data were collected from the single crystal using a KM-4 KUMA diffractometer, with Mo Kα radiation ($\lambda = 0.710\,73$ Å; graphite monochromator). The

0953-8984/98/245439+09$19.50

Table 1. Crystal data and a summary of the measurements for $[P(CH_3)_4]SbCl_6$.

Empirical formula	$[P(CH_3)_4]SbCl_6$
Formula weight	425.56
Temperature	293(2) K
Wavelength	0.710 73 Å
Crystal system	Triclinic
Space group	$P\bar{1}$
Unit-cell dimensions	
a (Å)	7.2050(10)
b (Å)	7.4110(10)
c (Å)	14.157(3)
α (deg)	89.68(3)
β (deg)	88.27(3)
γ (deg)	74.15(3)
Volume	726.9(2) Å^3
Z	2
Density (calculated)	1.944 Mg m^{-3}
Absorption coefficient	3.068 mm^{-1}
$F(000)$	408
Crystal size	$0.27 \times 0.24 \times 0.21$ mm
θ-range for data collection	2.86 to 30.06°
Index ranges	$-9 \leqslant h \leqslant 9, -10 \leqslant k \leqslant 10, -19 \leqslant l \leqslant 19$
Reflections collected	6663
Independent reflections	3901 ($R_{\rm int} = 0.0217$)
Refinement method	Full-matrix least-squares method, on F^2
Data/restraints/parameters	3901/0/161
Goodness of fit for F^2	1.013
Final R-indices ($I > 2\sigma(I)$)	$R_1 = 0.0294$, $wR_2 = 0.0665$
R-indices (all data)	$R_1 = 0.0528$, $wR_2 = 0.0733$
Extinction coefficient	0.0051(3)
Largest diffraction peak and hole	0.644 and -0.653 e Å^{-3}

lattice parameters were refined by setting angles of 25 reflections in the $18° < 2\theta < 30.5°$ range. A summary of the crystal data is presented in table 1.

Differential scanning calorimetry (DSC) measurements were carried out using a Perkin–Elmer DSC-7 differential scanning calorimeter. The DSC measurements were performed with rates ranging from 5 K min^{-1} to 20 K min^{-1}. The value of the temperature hysteresis ΔT was obtained by extrapolating the scanning rate to 0 K min^{-1}.

The linear thermal expansion was measured using a thermomechanical analyser (Perkin–Elmer TMA-7). The samples used in the measurements were prepared in the forms of thin plates of dimensions $5 \times 5 \times 1.5$ mm^3 (natural plates). The anomalies in the vicinity of the phase transitions were always reproducible within 10% for each sample. The accuracy of the thermal expansion determination was about 3%. The dilatometric measurements were performed during heating and cooling runs at a rate of 1 K min^{-1}.

The complex electric permittivity was measured using an HP 4285A Precision LCR Meter over the frequency range 75 kHz–30 MHz. The measurements were performed over the temperature range 300–410 K. The temperature of the specimen during the dielectric measurements was varied continuously at a rate of 0.1 K min^{-1} in the vicinity of T_c and 0.5 K min^{-1} elsewhere. The overall error for the real part of the complex electric permittivity was less than 5%.

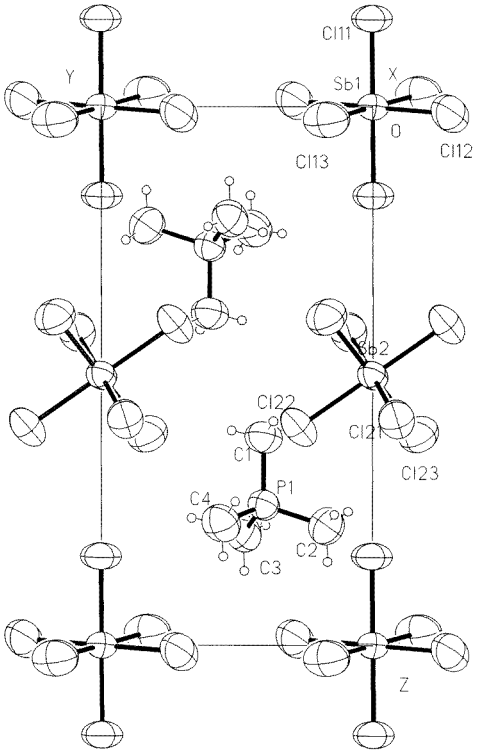

Figure 1. The projection along the *a*-axis of the crystal structure at room temperature (phase III) for $[P(CH_3)_4]SbCl_6$.

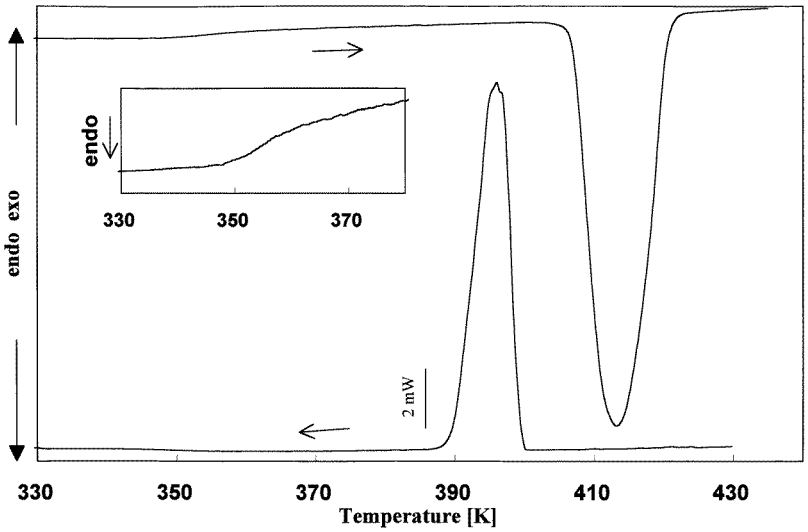

Figure 2. DSC curves obtained on heating and cooling for $[P(CH_3)_4]SbCl_6$. The inset is an enlargement of the results for the region of the low-temperature phase transition, which occurs at 350 K. (Scanning rate 5 K min^{-1}, sample mass 20.2 mg.)

The temperature dependence of the linear birefringence was studied using the rotating-analyser modulation method [8]. A 1 mW He/Ne laser served as a light source (λ = 632.8 nm). The light intensity measured had an amplitude proportional to $\sin\gamma$ (γ is the phase shift introduced by the optical retardation, $\gamma = (2\pi/\lambda)\Delta n\, t$, where λ is the wavelength, Δn is the linear birefringence and t is the thickness). The accuracy achieved for the birefringence change measurements was 10^{-6}. The cooling and heating rates in the phase transition region were both 0.05 K min^{-1}. For the birefringence measurements, plates that were 0.6 mm thick were used.

The low thermal conductivity of the samples (explained by the use of polycrystalline pressed samples in the dielectric measurements and the breaking of the crystal at the 405 K phase transition in the dilatometric experiment) is one reason for the inaccuracy of the values of the phase transition temperatures.

Table 2. Atomic coordinates (in units of 10^4) and equivalent isotropic displacement parameters (A^2 in units of 10^3) for $[P(CH_3)_4]SbCl_6$ at 293 K. U(eq) is defined as one third of the trace of the orthogonalized U_{ij}-tensor.

	x	y	z	U(eq)
Sb(1)	0	0	0	44(1)
Cl(11)	549(1)	20(1)	−1654(1)	67(1)
Cl(12)	2457(1)	−2858(1)	119(1)	86(1)
Cl(13)	2263(1)	1696(1)	240(1)	79(1)
Sb(2)	0	0	5000	43(1)
Cl(21)	2932(1)	−883(1)	5808(1)	64(1)
Cl(22)	−1051(1)	2718(1)	5957(1)	65(1)
Cl(23)	−1409(1)	−1699(1)	6085(1)	72(1)
P(1)	3791(1)	4004(1)	7398(1)	47(1)
C(1)	3614(4)	4009(4)	6148(2)	60(1)
C(2)	4946(5)	1692(4)	7786(2)	64(1)
C(3)	1431(4)	4756(4)	7921(2)	64(1)
C(4)	5154(5)	5577(5)	7734(2)	68(1)
H(11)	2909(53)	3158(51)	5970(26)	110(13)
H(12)	4842(51)	3647(50)	5849(25)	98(12)
H(13)	3060(51)	5190(48)	6023(24)	97(12)
H(21)	4958(48)	1662(45)	8447(25)	91(11)
H(22)	4341(52)	905(53)	7520(25)	100(12)
H(23)	6259(59)	1412(55)	7578(28)	125(15)
H(31)	814(45)	3941(43)	7773(22)	77(10)
H(32)	816(55)	5962(54)	7663(28)	121(14)
H(33)	1577(55)	4724(52)	8615(29)	112(13)
H(41)	5201(56)	5504(55)	8348(29)	120(14)
H(42)	6375(67)	5058(61)	7335(32)	142(17)
H(43)	4251(58)	6673(56)	7639(29)	118(14)

3. Results

3.1. X-ray data

This paper presents the crystal structure of TMPCA for phase III at room temperature. The crystal structure of phase III was solved by the Patterson method using the SHELXS 84 program. The two inequivalent isolated $SbCl_6$ octahedra are completely ordered. The

Table 3. Bond lengths (Å). (The symmetry transformations used to generate equivalent atoms are given in the footnotes.)

Sb(1)–Cl(13)	2.3478(10)
Sb(1)–Cl(13)[a]	2.3479(10)
Sb(1)–Cl(11)	2.3635(8)
Sb(1)–Cl(11)[a]	2.3635(8)
Sb(1)–Cl(12)[a]	2.3694(11)
Sb(1)–Cl(12)	2.3694(11)
Sb(2)–Cl(23)[b]	2.3575(10)
Sb(2)–Cl(23)	2.3575(10)
Sb(2)–Cl(21)	2.3626(9)
Sb(2)–Cl(21)[b]	2.3626(9)
Sb(2)–Cl(22)	2.3669(10)
Sb(2)–Cl(22)[b]	2.3669(10)
P(1)–C(3)	1.778(3)
P(1)–C(1)	1.778(3)
P(1)–C(2)	1.780(3)
P(1)–C(4)	1.791(4)
C(1)–H(13)	0.88(3)
C(1)–H(12)	0.94(3)
C(1)–H(11)	0.95(4)
C(2)–H(22)	0.91(4)
C(2)–H(23)	0.95(4)
C(2)–H(21)	0.94(3)
C(3)–H(31)	0.87(3)
C(3)–H(32)	0.96(4)
C(3)–H(33)	0.99(4)
C(4)–H(41)	0.87(4)
C(4)–H(43)	0.90(4)
C(4)–H(42)	1.01(5)

[a] $-x, -y, -z$.
[b] $-x, -y, -z+1$.

ordered $P(CH_3)_4^+$ groups occupy the vacant sites between the octahedral units. The projection along the *a*-axis of the crystal structure at room temperature (phase III) is shown in figure 1. The P(1) atom with four CH_3 groups forms the regular tetrahedral coordination. The final results of the refinement of the structure and the atomic coordinations are given in tables 1 and 2. Selected bond lengths are shown in table 3. In the monoclinic high-temperature phase (II) the $SbCl_6$ octahedra are characterized by large thermal motions, which means that they become disordered.

The full crystal structures for phase II, above 350 K, and for phase I, above 405 K, will form the subject of a separate paper. The preliminary structural results for phase II (373 K) are as follows: space group: $C2/m$; $a = 11.804$ (2) Å, $b = 8.854(2)$ Å, $c = 14.358(3)$ Å; $\beta = 91.4(3)^\circ$; $Z = 4$.

3.2. Differential scanning calorimetry measurements

Figure 2 shows a strong DSC peak at 406 K/400 K (±0.5 K) obtained during heating/cooling runs at the scanning rate of 5 K min^{-1}. The shape of the heat anomaly and the distinct thermal hysteresis (extrapolated to a scanning rate of 0 K min^{-1}, $\Delta T \approx 5$ K) clearly indicate the first-order nature of the phase transition. The enthalpy and entropy values of this transition are quite large, and amount to about 19.6 kJ mol^{-1} and 47.8 J mol^{-1} K^{-1},

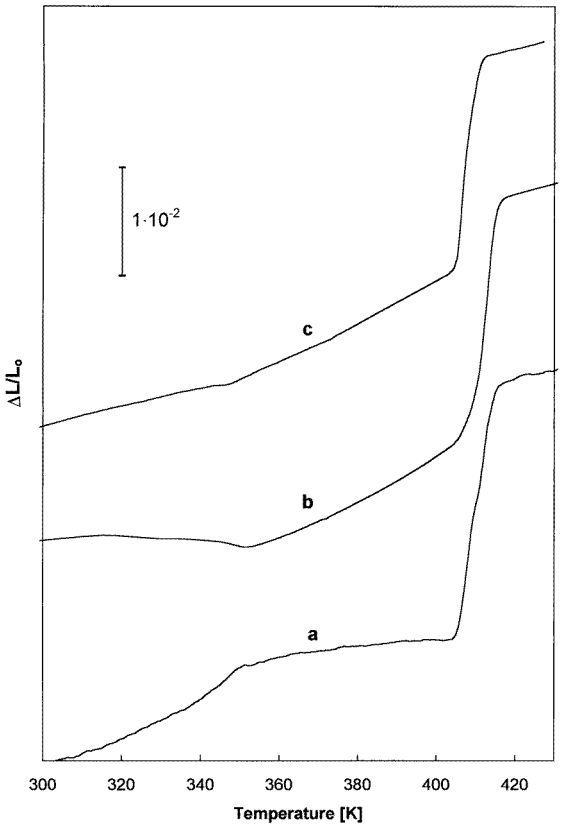

Figure 3. The temperature dependence of the linear thermal expansion $\Delta L/L$ measured along the *a*-, *b*- and *c*-axes at a rate of 1 K min^{-1} for $[P(CH_3)_4]SbCl_6$ (the notation for the axes is that for the monoclinic–paraelastic phase).

respectively. The thermal parameters suggest that this transition is likely to be of the order–disorder type. The inset in figure 2 presents the DSC curve in the vicinity of the 350 ± 2 K phase transition, confirming the continuous nature of the transition. These transitions are readily reversible as the material is cycled through the 300–420 K temperature range.

3.3. Dilatometric measurements

Figure 3 shows the thermal expansion of the TMPCA crystal on heating along the main crystallographic directions in the temperature range between 300 and 430 K. The notation for the crystallographic axes is according to the orientation of the crystals in the monoclinic phase, i.e. above 350 K. Distinct thermal anomalies at $T_{c2} = 350 \pm 1$ K and at $T_{c1} = 405 \pm 1.5$ K confirm the presence of the phase transitions found by the DSC method. At the low-temperature phase transition (350 K) only a change in the slope of the thermal dilation is observed, whereas a step-wise change in $\Delta L/L_0$ (where L_0 is the length of the sample at 300 K) was found at 405 K. In phase III, below T_{c2}, the averaged thermal expansion coefficient, $\bar{\alpha} = \Delta L/L_0\,\Delta T$, differs significantly for the three directions not only in value but also in sign. For direction $\boldsymbol{a}$, $\bar{\alpha}_a = 1.86 \times 10^{-4}$; for direction $\boldsymbol{b}$, $\bar{\alpha}_b = -1.2 \times 10^{-5}$; for direction $\boldsymbol{c}$, $\bar{\alpha}_c = 9.16 \times 10^{-5}$ K^{-1}. The corresponding values of $\bar{\alpha}$

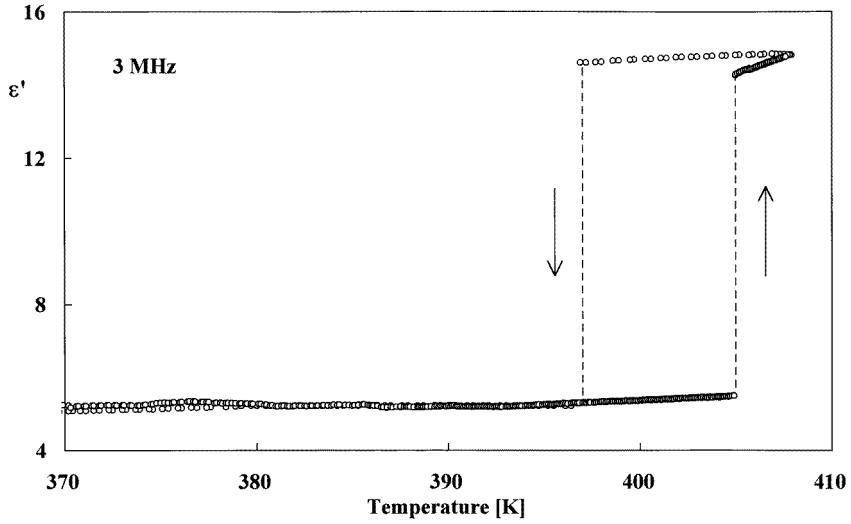

Figure 4. The temperature dependence of the real part of the complex electric permittivity at 3 MHz for the polycrystalline sample measured on heating and cooling at rates of 0.1 K min^{-1} close to $T_c = 405$ K and 0.5 K min^{-1} elsewhere.

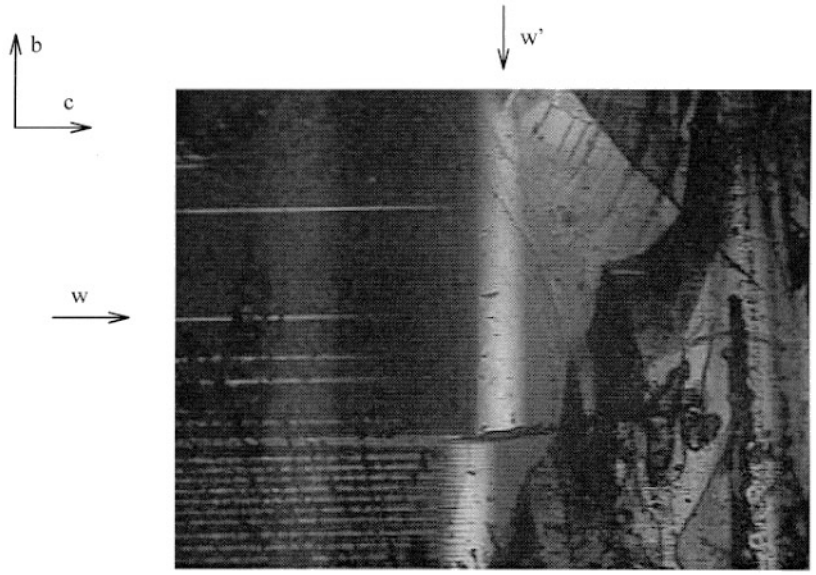

Figure 5. A micrograph of ferroelastic domains of $[P(CH_3)_4]SbCl_6$ between crossed polarizers taken along the *a*-axis at room temperature.

for phase II (above T_{c2}) are 5.04×10^{-5}, 1.65×10^{-4} and 1.62×10^{-4} K^{-1}, respectively. The change in $\Delta L/L_0$ in the vicinity of the high-temperature phase transition (405 K) is approximately the same for all directions and is equal to about 2×10^{-2}. The pressure coefficient of the 405 K phase transition estimated from the Clausius–Clapeyron relation, $dT_c/dp = \Delta V/\Delta S$, is equal to $+7.1$ K $kbar^{-1}$, where ΔV is the change in molar volume

and ΔS is the entropy change corresponding to the latent heat at T_c. The behaviour of the thermal expansion at T_{c1} (a step-wise change of $\Delta L/L_0$ and a distinct temperature hysteresis of -10 K) indicates the first-order nature of the II $\rightarrow$ I phase transition, which is in accordance with DSC results. It should be noted that the changes in the $\Delta L/L_0(T)$ curve occurring at the III $\rightarrow$ II phase transition are seen only for the first heating of the virgin sample.

3.4. Dielectric studies

The complex electric permittivity during heating and cooling scans measured at 3 MHz for polycrystalline pressed pellets with gold electrodes deposited on the surfaces is displayed in figure 4. A distinct rapid jump in the ε-value at 405 K/397 K (± 2 K) (heating/cooling) corroborates the first-order nature proposed for the phase transition visible in DSC and dilatometric measurements. The shape of the dielectric anomaly is characteristic of crystals exhibiting the 'rotational phase' at high temperatures. This is consistent with calorimetric studies suggesting a transition to a 'rotational phase' above 405 K. The low-temperature phase transition is inactive in dielectric measurements.

The rotational motions both of the tetramethylphosphonium cations and of the octahedral anions are believed to contribute to the order–disorder mechanism of the high-temperature phase transition at 405 K.

3.5. Optical observations

The virgin TMPCA samples were single domain. If a small mechanical stress is applied along the ***b***-direction, the crystals will show ferroelastic domains (in the *bc*-plane) at room temperature, as presented in figure 5. The domain walls of type w ran perpendicular to the monoclinic *b*-axis whereas the domain walls of type w′ (the wide bright region) are parallel to this axis. On heating, the single-domain samples change to multidomain ones, and then at 350 ± 0.5 K the domains disappear. A phase front was observed during the 405 K phase transition, corroborating the first-order character proposed for this transition.

3.6. Birefringence measurements

As seen in figure 6, the linear birefringence Δn_a (where $\Delta n_a = n_b - n_c$ and is equal to 4.4×10^{-3} at room temperature) changes continuously around 350 K, confirming strongly the second-order character of the ferroelastic–paraelastic phase transition. The deflections of the birefringence $|\delta\, \Delta n_a|$ for the ferroelastic phase from those of the extrapolated high-temperature paraelastic phase are also illustrated in figure 6.

The indicatrix rotation was observed only in the *bc*-plane. The extinction position changes monotonically from 11° at room temperature to 0° at T_c (with respect to the *ab*-plane). This diminishes the observed linear birefringence changes by up to about 10% but does not affect the character of the curve. No significant indicatrix rotation in the *ac*- and *ab*-planes was noticed ($\Delta\varphi < 1^\circ$).

4. Conclusion

The $[P(CH_3)_4]SbCl_6$ crystal has been shown to undergo a second-order ferroelastic–paraelastic phase transition at 350 K, and then a first-order transition at 405 K. The ferroelastic phase transition is characterized by a symmetry change from the monoclinic

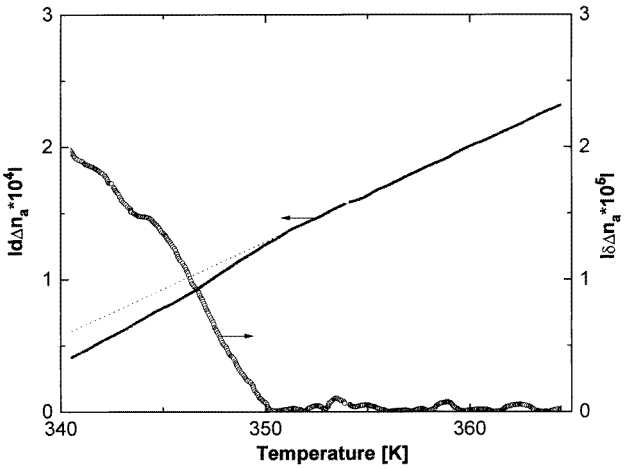

Figure 6. The linear birefringence, $\mathrm{d}\,\Delta n_a$ (left-hand scale), behaviour of $[P(CH_3)_4]SbCl_6$ along the a-axis and its increment, $\delta\,\Delta n_a$ (right-hand scale), in the vicinity of the ferroelastic–paraelastic phase transition measured on cooling at a rate of 0.05 K min^{-1}.

space group $C2/m$ to the triclinic space group $P\bar{1}$. The domain structure of $[P(CH_3)_4]SbCl_6$ observed at room temperature is interpreted on the basis of Sapriel's method [9] by taking into account the symmetry change from $2/m$ to $\bar{1}$.

Acknowledgment

This work was supported by Polish State Committee for Scientific Research (project register No 3T09A 093 10).

References

[1] De Beer W H J, Heyns A M, Richter P W and Clark J B 1980 *J. Solid State Chem.* **33** 283
[2] Sato S, Kondo M, Ikeda R and Nakamura D 1989 *Ber. Bunsenges. Phys. Chem.* **93** 450
[3] Reynhardt E C and Rash P S 1981 *J. Magn. Reson.* **42** 88
[4] Howe R F and Taylor M J 1987 *Spectrochim. Acta* A **43** 73
[5] Zeegers Th and Bator G 1996 *Vibrat. Spectrosc.* **13** 41
[6] Kruger F J and Schmidt A 1976 *Z. Anorg. Allg. Chem.* **427** 55
[7] Jakubas R, Ciąpała P, Pietraszko A, Zaleski J and Kusz J 1998 *J. Phys. Chem. Solids* at press
[8] Wood I G and Glazer A M 1980 *J. Appl. Crystallogr.* **13** 224
[9] Sapriel J 1975 *Phys. Rev.* B **12** 5128